ChemElectroChem

Research Article
doi.org/10.1002/celc.202400070

Chemistry Europe
European Chemical Societies Publishing

www.chemelectrochem.org

# Increasing Activity of Trimetallic Oxygen Reduction PtNiMo/C Catalysts Through Initial Conditioning

Bilal Danisman,[a] Gui-Rong Zhang,[a, b] Adrian F. Baumunk,[a, c] Juntao Yang,[d] Olaf Brummel,[d] Philipp Darge,[e] Dominik Dworschak,[e] Karl J. J. Mayrhofer,[e] Jörg Libuda,[d] Xin Zhou,[f] Mingjian Wu,[f] Erdmann Spiecker,[f] Marc Ledendecker,[a, g] and Bastian J. M. Etzold*[a, c]

This study investigates the importance of preconditioning in Pt-alloy catalysts for oxygen–reduction reactions. Previous research indicated that slower scanning rates during preconditioning initially boost activity, but this is followed by a rapid decline. The study reveals the required number of cycles to achieve the first constant steady state activity in PtNiMo/C catalysts when using slower scanning rates during preconditioning. It also highlights the resulting activity differences. Remarkably, a catalyst preconditioned with 150 slow cycles showed an activity of approximately 1.25 mA cm$^{-2}$ at 0.90 $V_{RHE}$, significantly higher than one preconditioned at a fast rate (0.82 mA cm$^{-2}$). Both ex–situ and in–situ analyses revealed that Pt, along with Ni, was leached during pretreatment. At slower scan rates of 20 mV s$^{-1}$, the dissolved Pt redeposited as highly active, small-sized clusters or single atoms. Fast scan rates of of 500 mV s$^{-1}$, in contrast, resulted in fewer such clusters. Accelerated stress tests up to 1.10 $V_{RHE}$ confirmed the high stability of these clusters, demonstrating a substantial activity increase even after 24,000 cycles.

## Introduction

Platinum–based catalysts are state–of–the–art for oxygen reduction reaction (ORR) in proton–exchanged membrane fuel cells (PEMFC). However, their performance is limited by sluggish kinetics at the cathode and poor stability above 1.0 $V_{RHE}$. Therefore, intensive efforts are directed to improve their activity and durability.[1–5] Various strategies, from alloying to nano structuring, have been employed to boost the specific activities of Pt-based catalysts.[6–16] Strasser et al.[17] found that an octahedral-shaped PtNi nanoparticle with Mo incorporation featuring Pt–rich edges and Ni–rich facets, demonstrates enhanced ORR performance.[17]

Despite advances in activity, the stability of alloy catalysts beyond 0.95 $V_{RHE}$ remains a challenge.[18] Octahedral PtNi nanoparticles with (111)-facets exhibit metal leaching, causing decreasing activity due to Pt oxidation.[18,19] Alloying with a third metal (e.g., Mo,[17,20,21,22] Co,[23] Rh[24]) can improve stability. However, trimetallic PtNiMo/C catalysts show ongoing dissolution of transient metals (Ni, Mo).[25,19] The dynamics of alloy and nanostructure catalysts, originating from Pt3M (M = transition metals) studies, pose challenges in assessing activity and pre–activation procedures in classical rotating disc electrode (RDE) testing.[26,27] In the past, changes in the electrochemically active surface area (ESCA) during pretreatment were mainly used to ensure the completion of initial restructuring of the alloy catalyst.[17,22] We showed in our previous work, that strong activity changes occur during the initial preconditioning of a trimetallic PtNiMo/C catalysts at slow scan rates (20 mV s$^{-1}$). Commonly a faster scanning with 100 to 500 mV s$^{-1}$ is

[a] B. Danisman, Prof. Dr. G.-R. Zhang, A. F. Baumunk, Prof. Dr. M. Ledendecker, Prof. Dr.-Ing. B. J. M. Etzold
Department of Chemistry, Ernst-Berl-Institute for Technical and Macromolecular Chemistry
Technical University of Darmstadt
64287 Darmstadt, Germany
E-mail: bastian.etzold@tu-darmstadt.de
Homepage: www.etzoldlab.de

[b] Prof. Dr. G.-R. Zhang
School of Chemical Engineering and Technology
Tiangong University
BinShuiXi Road 399, Tianjin 300387, China

[c] A. F. Baumunk, Prof. Dr.-Ing. B. J. M. Etzold
Department of Chemical and Biological Engineering, Power-to-X Technologies
FAU Erlangen-Nürnberg
Egerlandstr. 3, 91058 Erlangen, Germany

[d] J. Yang, Dr. O. Brummel, Prof. Dr. J. Libuda
Erlangen Center for Interface Research and Catalysis
FAU Erlangen-Nürnberg
Egerlandstr. 3, 91058 Erlangen, Germany

[e] P. Darge, Dr. D. Dworschak, Prof. Dr. K. J. J. Mayrhofer
Forschungszentrum Jülich GmbH
Helmholtz-Institute Erlangen-Nürnberg for Renewable Energy (IEK-11)
Cauerstr. 1, 91058 Erlangen, Germany

[f] Dr. X. Zhou, Dr. M. Wu, Prof. Dr. E. Spiecker
Institute of Micro- and Nanostructure Research (IMN) & Center for Nanoanalysis and Electron Microscopy (CENEM), Interdisciplinary Center for Nanostructured Films (IZNF), Department of Materials Science and Engineering, Friedrich-Alexander-Universität Erlangen-Nürnberg Cauerstrasse 3, 91058 Erlangen Germany

[g] Prof. Dr. M. Ledendecker
Sustainable Energy Materials, Campus Straubing for Biotechnology and Sustainability
Technical University of Munich, Schulgasse 22, 94315 Straubing Germany

Supporting information for this article is available on the WWW under https://doi.org/10.1002/celc.202400070

employed during the pretreatment (see Supporting Information Table S1).[28] The ORR activity increased by a factor of 2.3 for the first ten cycles, while the ECSA increased only by a factor of 1.2. The activity increase could be correlated to the surface restructuring and the formation of larger Pt facets as well as of small Pt clusters. We also reported a strong activity decrease with increasing preconditioning cycle number and didn't expand the study to identify after which cycle number a first constant activity for these alternative slow preconditioning cycles is reached. Thus, it is an open question if the type of pretreatment with respect to scanning rate and type of atmosphere (inert gas ($N_2$/Ar) or $O_2$) affects the initial restructuring and thus on the resulting steady state activity and how many pretreatment cycles are needed to reach this initial steady state.

In this study, we employ the same literature known PtNiMo/C alloy catalyst[22,29,28] which showed these strong activity dynamics during preconditioning, to answer these open questions. We applied 100 and 150 cyclic slow scanning cycles as well as 300 chronoamperometry steps as preconditioning. To be able to judge if really a constant initial activity is reached after preconditioning, we studied different testing protocols of several ORR testing cycles and electrolyte refreshing, which allow to see activity changes over these cycles if no steady state is reached. Electrochemical infrared reflection absorption spectroscopy (EC-IRRAS) and scanning transmission electron microscopy with energy dispersive x-ray spectroscopy (STEM-EDXS) as well as further characterization are employed to gain fundamental insights on the catalyst restructuring. No difference was found between using inert gas or $O_2$ saturated electrolyte, but the slow scanning precondition resulted in approx. 50% higher activity compared to classical fast scanning. This can be attributed to the formation of small platinum clusters during the preconditioning. Accelerated stress testing showed, that these cluster are stable.

## Results and Discussion

### Assessing Initial Steady State Activity for Different Conditioning Protocols

To be able to compare the influence of the initial conditioning on activity, first a suitable measurement protocol to gain initial steady state activities needs to be found. Based on our previous experience[28], constant ECSA during CV cycling is not a suitable indicator and an asymptotic progression of specific activities through increasing conditioning cycle numbers result not achieving steady state (see Supporting Information Figure S6). Furthermore, the alternative conditioning protocols studied also contain ORR polarization cycling, where no ECSA change can be determined. To identify if an initial steady state activity is obtained after conditioning, several polarization curves are recorded in series and the electrolyte is refreshed after either 5, 10 or 15 polarization curves. This is done and compared for different conditionings described in the experimental sections and carried out prior.

Before discussing the differences in activity determined after the conditioning, an insight into the activity development during the conditioning cycles is given for Conditioning 2 carried out in $O_2$, where activity can be deduced. Conditioning 2 was carried out for 100 or 150 cycles and with and without 10 or 15 Conditioning 1 cycles. The results are depicted in Figure 1. It needs to be noted that the "specific activity_cyclic voltammetry$_{end}$" (SA_CV$_{end}$) values recorded at 0.90 $V_{RHE}$ corresponds to the ECSA determined after the end of the full conditioning protocol as no ECSA is determined at each cycle.

In addition, all further SA values are equally defined as "SA_CV$_{end}$". Also, for a better understanding, the notation will be defined as followed: E.g., "C1-10-N2_C2-100-O2", means a

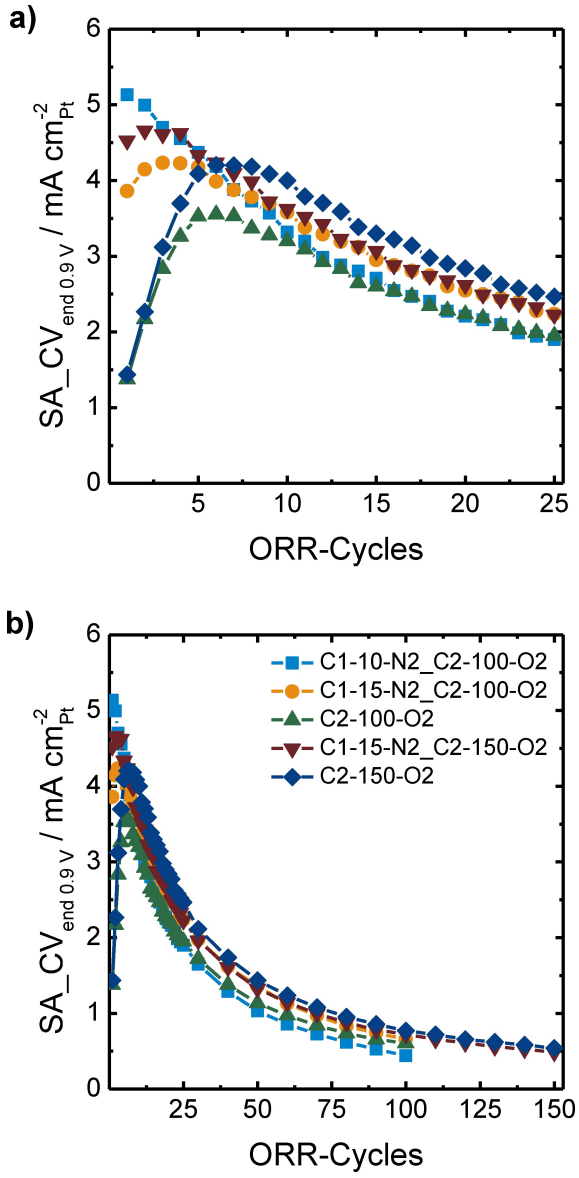


**Figure 1.** ORR activities determined during Conditioning 2 after different cycles in $O_2$. a) The initial activity development within 25 ORR-cycles and b) for the overall picture up to 100 or 150 Conditioning 2 cycles, respectively. Conditioning 1 recorded at 500 mV s$^{-1}$ in $N_2$, Conditioning 2 at 20 mV s$^{-1}$ in $O_2$ with 1600 rpm rotation in saturated 0.1 M $HClO_4$ solution. Potential range: 0.05–1.20 $V_{RHE}$.

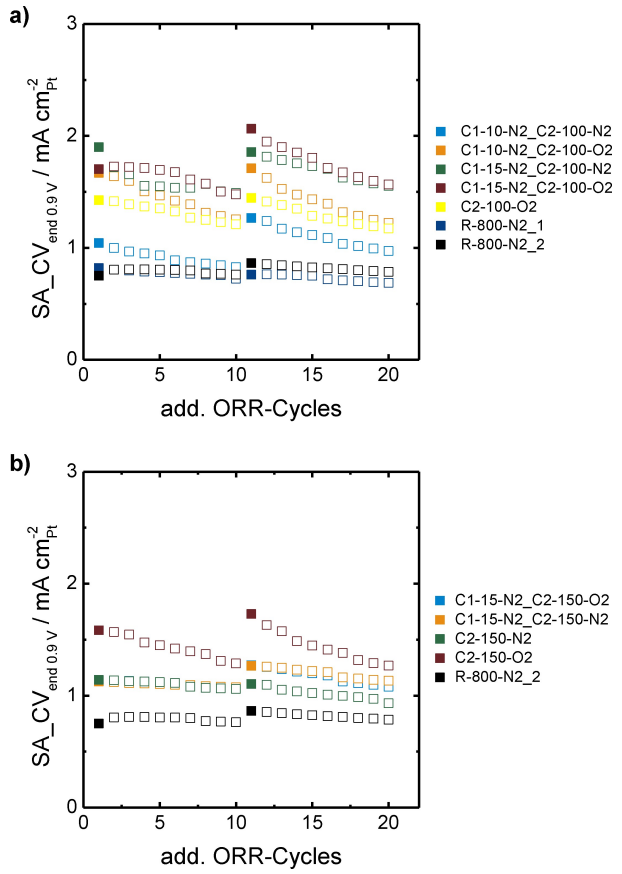


**Figure 2.** 20 Specific activities recorded with additional ORR-cycles after various conditionings. Electrolyte was refreshed before the 1st and 11th add. ORR-cycle and measurements starting with fresh electrolyte are given by filled symbols. a) After 100 Conditioning 2 cycles in $N_2$ or $O_2$; b) After 150 Conditioning 2 cycles in $N_2$ or $O_2$. For a) and b) the potential range is 0.05–1.20 $V_{RHE}$ at 20 mV s$^{-1}$ for Conditioning 2 and at 500 mV s$^{-1}$ for Conditioning 1 and Reference, respectively. SA recorded during additional ORR cycles with 20 mV s$^{-1}$ and 1600 rpm in $O_2$-saturated 0.1 M $HClO_4$ solution.

Conditioning 1 with 10 cycles in $N_2$ followed by 100 Conditioning 2 cycles in $O_2$, "R-800-N2" are 800 cycles in $N_2$ for the Reference method and "C3-300-N2" are 300 Conditioning 3 steps in $N_2$ for the chronoamperometric conditioning, respectively.

Similar to our previous study, strong activity changes are observed for the first 25 ORR-cycles (Figure 1a).[28] Following the trend for more cycles a strong decay of the interim high activity is observed for all conditioning protocols (Figure 1b) and activities ranging from 0.44 to 0.54 mA cm$_{Pt}^{-2}$. A similar trend of specific activity is also seen at values recorded at 0.95 $V_{RHE}$ (see Supporting Information Figure S7 and S8). As these activities determined without electrolyte refreshing, they give only a first indication when initial steady state activities can be expected.[28,30]

Figure 2 shows 20 additional ORR polarization cycles after different conditionings and now with electrolyte refreshing prior the 1st and 11th additional ORR cycle. For 100 Conditioning 2 cycles (Figure 2a) and 150 Conditioning 2 cycles (Figure 2b) similar results are obtained. The polarization curves without electrolyte refreshing show a constant lowering of the activity, which is interestingly lower for the Reference condition protocol. Nevertheless, after electrolyte refreshing it gets clear that the 11th additional polarization curves show no deactivation compared to the 1st additional one, even showing a slight activity increase. More importantly, the different conditionings result in strongly different activities. Figure 3 (and Figure S9 at 0.95 $V_{RHE}$ in the Supporting Information) compares the activities determined within the 1st and 11th additional cycle directly after electrolyte refreshing, which range from 0.76 to 2.06 mA cm$_{Pt}^{-2}$.

Among the different conditioning protocols used, no clear trend for difference in activity can be deduced. But clearly the commonly employed reference method led to the lowest activities and the conditioning seems to show a strong influence on the achieved activity. In addition, we noticed that a previous Conditioning 1 with fast and short potential cycling

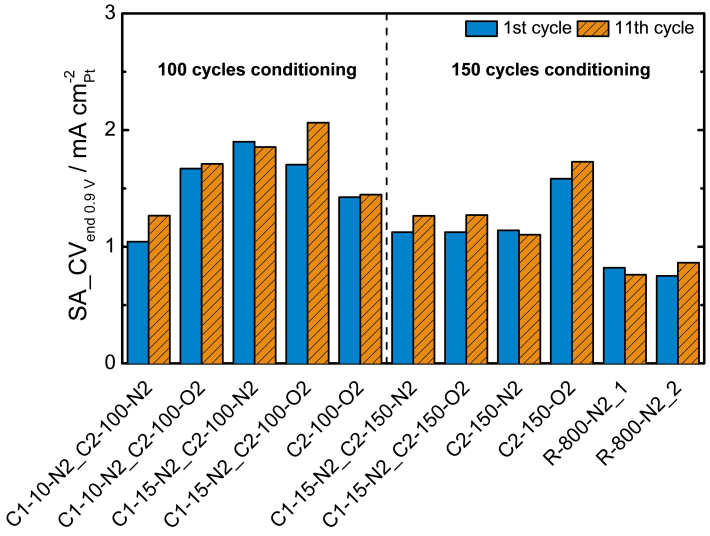


**Figure 3.** Representation of the SA at 1st and 11th ORR-cycle from 100 and 150 cycles of conditioning, respectively. Potential range: 0.05–1.20 $V_{RHE}$ at 20 mV s$^{-1}$ for Conditioning 2, at 500 mV s$^{-1}$ for Conditioning 1 and Reference, respectively. Activity recorded at 20 mV s$^{-1}$ in $O_2$-saturated 0.1 M $HClO_4$ solution.

at 500 mV s$^{-1}$ does not have any positive impact and was skipped for the experiments presented subsequently. Also, lower activities are obtained for 150 cycles compared to 100 cycles. Therefore, equilibration of the catalyst seems still to take place until 150 cycles, which are thus employed for the subsequent studies.

As the reversible deactivation without electrolyte refreshing is unexpectedly high, a proper protocol to check if the activity has equilibrated after the conditioning phase which includes several electrolyte refreshing needs to be determined. Therefore, first a new data set was prepared with 25 additional polarization curves after the conditioning but electrolyte refreshing prior to the 1$^{st}$, 6$^{th}$, 11$^{th}$, 16$^{th}$ and 21$^{st}$ additional cycle. The results are given in Figure 4. The Reference Conditioning

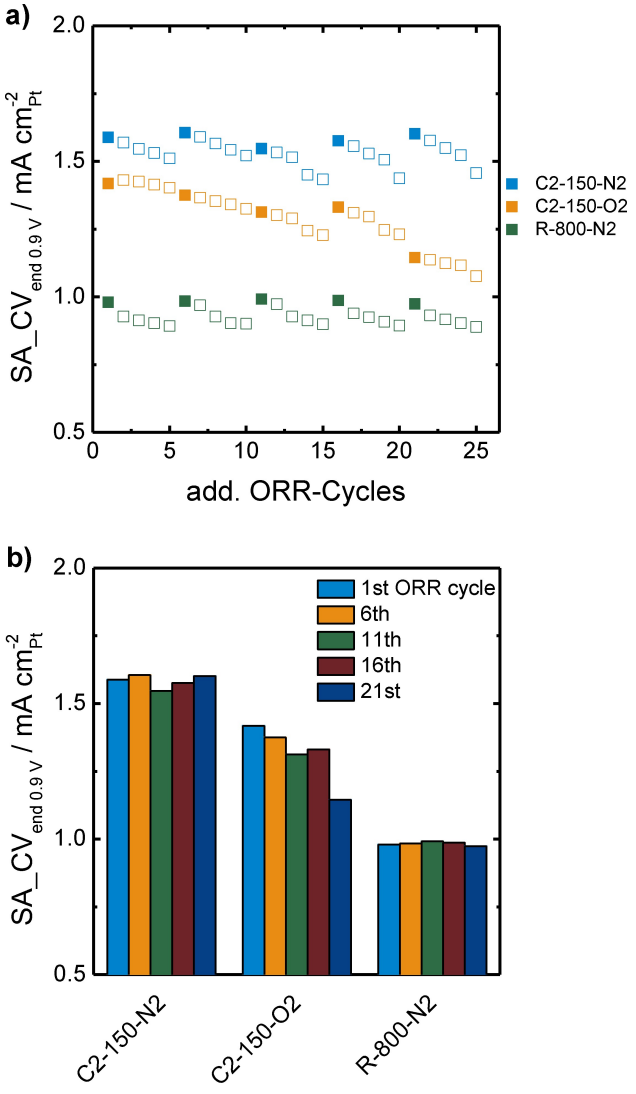


**Figure 4.** Specific activities recorded with additional ORR-cycles for 150 conditioning cycles with Conditioning 2 in $N_2$ or $O_2$ as well as the Reference Conditioning and with electrolyte refreshing before the 1$^{st}$, 6$^{th}$, 11$^{th}$, 16$^{th}$ and 21$^{st}$ additional ORR-cycle. a) SA progresses during additional ORR-cycles with cycles after electrolyte refreshing highlighted with full symbols and b) activities at 1$^{st}$, 6$^{th}$, 11$^{th}$, 16$^{th}$ and 21$^{st}$ ORR-cycle after electrolyte refreshing, respectively. Potential range: 0.05–1.20 $V_{RHE}$, scan–rate: 20 mV s$^{-1}$ in saturated 0.1 M $HClO_4$ solution. Reference method recorded at 500 mV s$^{-1}$.

results in again the lowest SA of 0.98 mA cm$^{-2}$ at the 1$^{st}$ ORR-cycle, which remains constant over five–time electrolyte refreshing (Figure 4b). Both, Conditioning 2 in $N_2$ and $O_2$ show an outcome at an activity range between 1.25–1.60 mA cm$^{-2}$. Conditioning 2 in $N_2$ shows almost constant activity for the 5 measurements with fresh electrolyte, while Conditioning 2 in $O_2$ shows a decay in activity. All ORR cycles carried out within the same electrolyte show a drop in activity, which can be reversible after electrolyte refreshing. Thus, it can be concluded that only activities determined after electrolyte refreshing give meaningful results, even for small cycle numbers. Furthermore, it became clear that several measurements with fresh electrolyte are necessary before judging if the catalyst restructuring has already stabilized and shows stable activity. Combining both can lead to valid data.

Following these insights, the final protocol for determining activity after different conditionings was defined and employs 45 additional ORR polarization curves after conditioning and electrolyte refreshing prior to the 1$^{st}$, 16$^{th}$ and 31$^{st}$ cycle. Thus, three data points after electrolyte refreshing can be compared but the catalyst has also 15 cycles time to show changes and prove that steady activity was reached. Results obtained when employing this final protocol are given in Figure 5. Again, the Reference Conditioning shows the lowest activity. Interestingly, the measurement for the 1$^{st}$ additional ORR-cycle seemed to show – despite electrolyte refreshing – lower activity, which recovered for the 16$^{th}$ and 31$^{st}$ additional ORR cycle to approx. 0.82 mA cm$^{-2}$. This gives a further motivation for the several electrolyte refreshments used. As expected from the prior results, higher SA values are observed for Conditioning 2 in $N_2$ and $O_2$ in the range of 1.13–1.42 mA cm$^{-2}$. Conditioning 2 in $O_2$ resulted in nearly unchanged activities after the 3 cycles, after refreshing the electrolyte and thus initial steady state activities. However, a continuous decrease is now seen for Conditioning 2 in $N_2$ (Figure 5b) and steady state activity is not reached.

The conditioning of the catalyst shows clear influence on the gained activity and is an attractive new tool to enhance it. Previous conditionings used potential cycling between 0.05–1.20 $V_{RHE}$. Another option is square wave potential cycles with potential jumps, which are e.g., more common in membrane electrode assembly experiments. We investigated the effect of such steps using a new conditioning. In this Conditioning 3 we applied 300 chronoamperometric steps between 0.60–1.00 $V_{RHE}$, 0.65–1.00 $V_{RHE}$, or 0.70–1.00 $V_{RHE}$ with a dwell time of 57.5 sec at each potential step. The dwell time thereby was chosen to be in total the same as during the CV cycling time. The activity determined with addition 45 ORR cycles and 3 times electrolyte refreshing are given in Figure 6. Differences in the square wave cycling in comparison to the triangular protocol can be seen in the activity progress after conditioning (Figure 6a). Here, for all potential ranges, a sharp SA increase in the first 15 ORR-cycles occurs. Later, a strong deactivation can be seen, also after electrolyte refreshing. The restructuring reported during the first 25 ORR cycles[28] seems to take place. Thus, Conditioning 3 seems to be in an earlier stage of the catalyst equilibration and still strong activity changes are observed. No steady state activity could be achieved for all three Conditioning 3 studied.

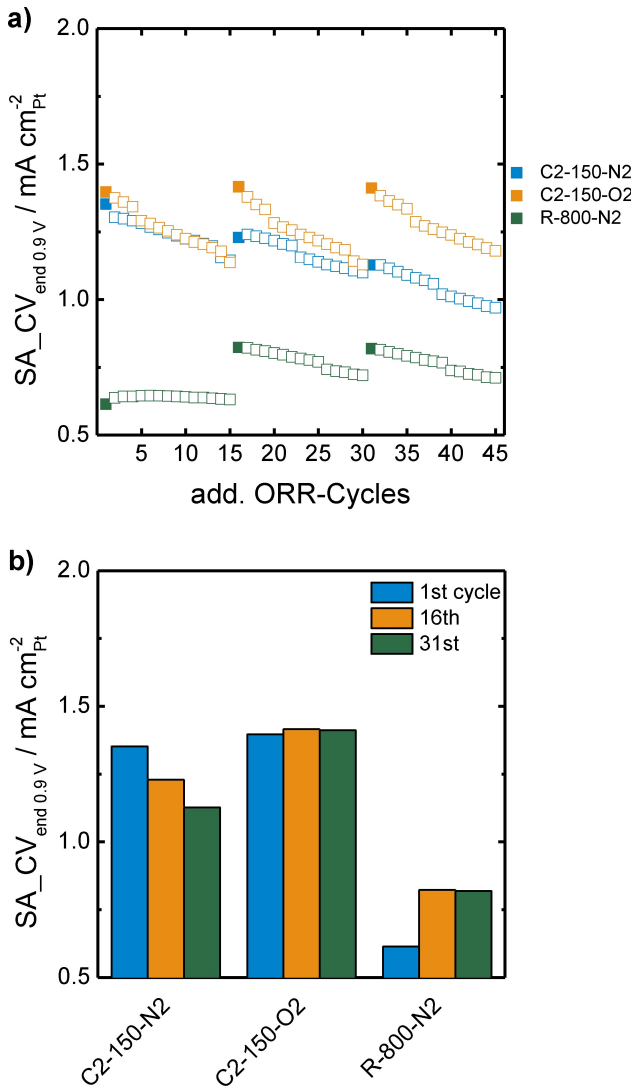


**Figure 5.** a) Activity records of three time 15 ORR cycles after 150 Conditioning 2 cycles and b) selected SA values at 1st, 16th and 31st cycle after refreshing electrolyte every 15 cycles. Potential range: 0.05–1.20 $V_{RHE}$, scan–rate: 20 mV $s^{-1}$ at 1600 rpm in $O_2$-saturated 0.1 M $HClO_4$ solution. Reference method at 500 mV $s^{-1}$.

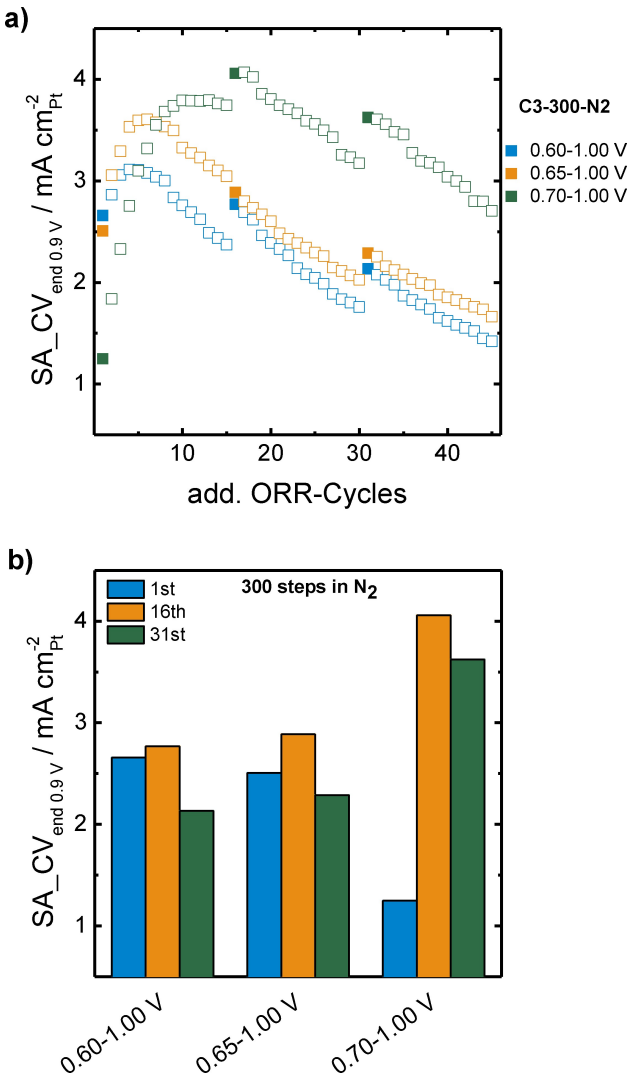


**Figure 6.** Activity records after 300 chronoamperometric conditioning steps in square wave potential ranges between 0.60—, 0.65— and 0.70–1.00 $V_{RHE}$ in $N_2$, respectively. a) SA progress during three times 15 ORR-cycles and b) activities at 1st, 16th and 31st ORR-cycle after electrolyte refreshing. Dwell time at each potential limit: 57.5 sec; ORR potential range: 0.05–1.20 $V_{RHE}$ at 20 mV $s^{-1}$ and 1600 rpm in $O_2$-saturated 0.1 M $HClO_4$ solution.

Probably this milder conditioning could allow more control. The variation of the lower potential shows similar results for 0.60 and 0.65 $V_{RHE}$, while for 0.70 $V_{RHE}$ higher activities are obtained. It is speculated that for 0.70 $V_{RHE}$, the initial activation phase seems to be in an earlier phase. Very likely, the higher potential leads to less reduction of platinum oxide and leached species.

### Studies on Active Site Changes During Conditioning

The study showed that activities are influenced strongly by the conditioning and pronounced increased activities can be gained when varying the conditioning protocol compared to the state of the art. To gain insights how the catalyst changes during the conditioning and which leads finally to this increase in activities, the metal dissolution was studied and CO stripping experiments as well as electrochemical in-situ IR spectroscopy were carried out and supported by additional TEM characterization.

We probed the active sites of the electrocatalysts after different conditioning procedures using CO stripping by CV and EC-IRRAS. Specifically, we compare the conditioning procedure carried out in Ar atmosphere C2-150-Ar and under oxygen saturated conditions C2-150-O2. Note that these treatments showed pronounced differences in the specific activity (see Figure 3). As a reference, we choose the conditioning procedure R-800-Ar, which had the lowest specific activity of the samples tested. We illustrate the experimental procedure in Figure 7a. After conditioning (i), we adsorbed CO on the catalyst (ii), removed CO from the solution by purging with Ar (iii), and measured CV or EC-IRRAS in a potential range between 0.05 and 1.2 $V_{RHE}$ (iv) (see experimental section for further details). It should be emphasized that CO treatment gives rise to the

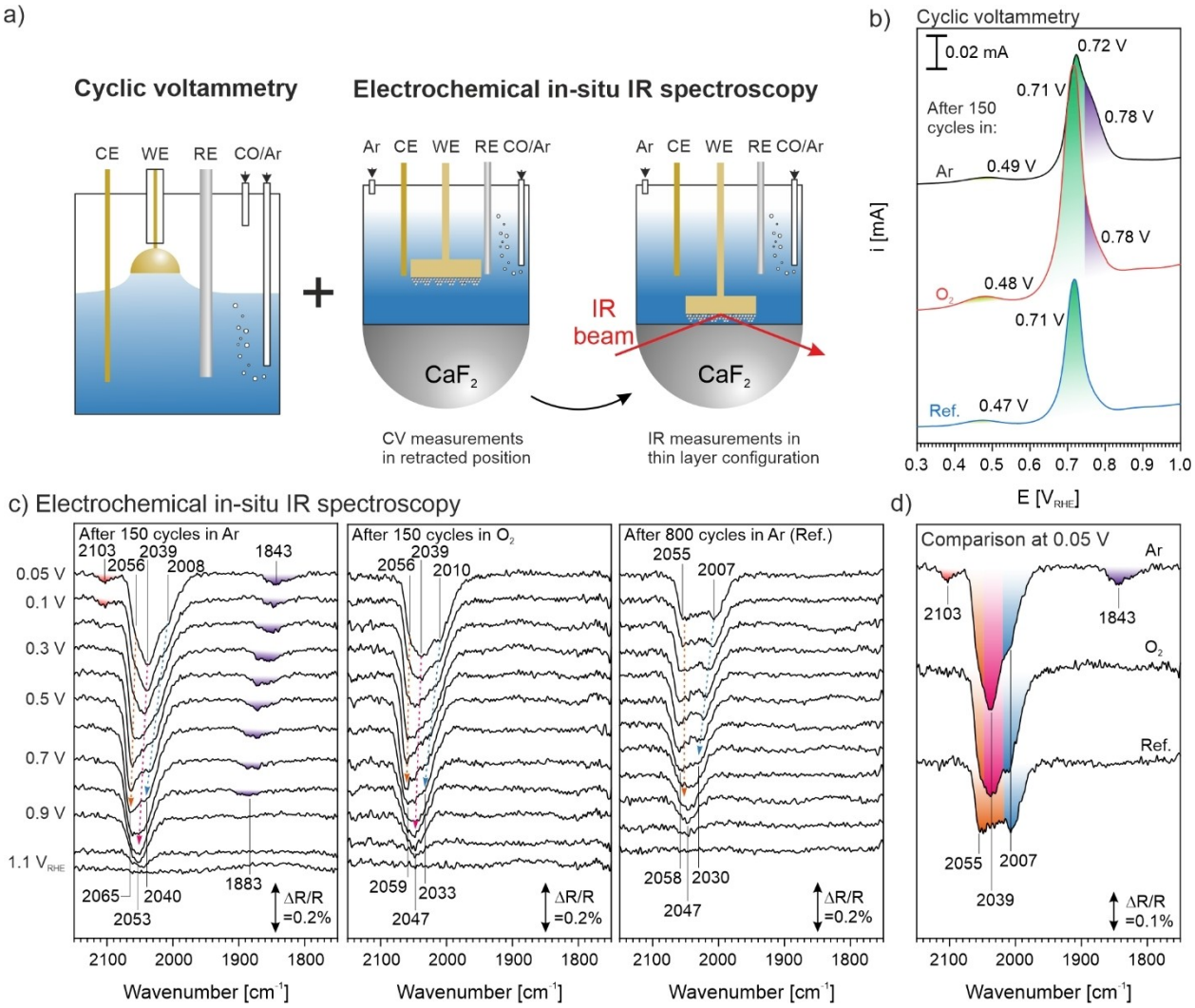


**Figure 7.** CO stripping experiment on PtNiMo/C catalyst with CV and EC-IRRAS; a) experimental procedure, b) cyclic voltammograms, c) potential dependent IR spectra and d) Comparison of IR spectra from different samples measured at 0.05 $V_{RHE}$. All measurements were performed in 0.1 M $HClO_4$. IR spectra are referenced to a spectrum at 1.2 $V_{RHE}$ recorded after CO stripping.

formation of small particles (see Figure S12) and, therefore, we show only the first cycle of CO oxidation. In the CV, we observe a sharp peak at ~0.71 $V_{RHE}$ (dark green) as the dominant feature (main peak), a smaller pre–peak (light green) at ~0.48 $V_{RHE}$, and an additional feature at ~0.78 $V_{RHE}$ (purple) for all treated samples. The feature at 0.78 $V_{RHE}$ appears as a shoulder of the main peak and is particularly pronounced for the two samples treated with Conditioning 2. The ratio between the shoulder at 0.78 $V_{RHE}$ and the main peak at 0.71 $V_{RHE}$ also depends on the atmosphere in which the conditioning was performed and is highest for cycling in Ar atmosphere. In addition, we observe pronounced differences in the total charges obtained during CO stripping, which follows C2-150-O2 (0.480 mC) ⩾ C2-150-Ar (0.287 mC) > R-800-Ar (0.266 mC) (see Figure S11). Note that the trend confirms the specific activity shown in Figure 3.

We assign the peak at ~0.71 $V_{RHE}$ to CO adsorption on Pt facets[28] and the pre-peak at ~0.48 $V_{RHE}$ to CO adsorption on Pt sites near $NiO_x$, as described by Strasser et al.[31] We attribute the shoulder at 0.78 $V_{RHE}$ to CO adsorbed on small Pt clusters, following the assignment in our previous work.[28] Note that a shift to higher CO oxidation potentials for small particles has been previously reported by other groups as well.[32,33] However, the formation of these clusters depends on the conditioning protocol used. While the highest number of small clusters are formed for C2-150-Ar, only a very small fraction of clusters is found after the extensive cycling in R-800-Ar. The correlation of the charges obtained in CO stripping with the specific activity obtained during ORR suggests that the specific activity is determined by the availability of active sites.

To gain further insight, we performed EC-IRRAS using an identical experimental procedure. The potential dependent IR spectra of CO stripping on the differently conditioned samples are shown in Figure 7c. Note that all IR spectra are difference spectra with respect to a CO-free spectrum recorded at 1.2 $V_{RHE}$. In these spectra, negative bands (oriented downwards) indicate adsorbed species present at the particular potential. For the sample pretreated with C2-150-Ar, we identify three clearly separated bands at 0.05 $V_{RHE}$, two smaller bands at 2103 and

1843 $cm^{-1}$, and the most intense band at 2039 $cm^{-1}$, which has a complex shape. At $\geq$ 0.3 $V_{RHE}$ we observe the disappearance of the band at 2103 $cm^{-1}$ and the shape of the band at 2039 $cm^{-1}$ changes several times. Note that we will discuss the shape and the potential dependent development of this band in more detail at later point. The bands at 2039 (including their different contributions) and 1843 $cm^{-1}$ shift to the blue with increasing potentials and disappear at 1.1 and 0.9 $V_{RHE}$, respectively. We assign the bands at 2039 and 1843 $cm^{-1}$ to adsorbed CO in on top ($CO_t$) and bridge bonded ($CO_b$) positions.[34] The origin of the band at 2103 $cm^{-1}$ is still debated. Our previous work suggests the formation of carbonyl–like Pt species.[35] However, we cannot exclude the formation of strongly bound CO on oxidized Pt, as suggested by Christopher et al., which might be stabilized by $NiO_x$ species.[36,37] The potential shift observed for the $CO_t$ and $CO_b$ band is attributed to the Stark effect.[38]

In the next step, we will discuss the shape of the $CO_t$ band and its potential dependent evolution. Beside the maximum at 2039 $cm^{-1}$, there is a blue- and a redshifted shoulder at 2055 and 2008 $cm^{-1}$ at 0.05 $V_{RHE}$, respectively. Note that there might be additional contributions that cannot be resolved. At 0.3 $V_{RHE}$, the blue–shifted shoulder becomes the dominating species. Above 0.9 $V_{RHE,}$ the blue and red–shifted contributions disappear, leaving a contribution at 2053 $cm^{-1}$, which is fully oxidized at $\geq$1.1 $V_{RHE}$. We assign the contribution at 2055 $cm^{-1}$ to $CO_t$ adsorbed on facet sites, the contribution at 2039 $cm^{-1}$ to a combination of low coordinated adsorption sites[39] and small Pt clusters[28,39] and the contribution at 2008 $cm^{-1}$ to Pt atoms neighboring the alloying metals.[28,35] We attribute the remaining band at 2053 $cm^{-1}$ to the presence of small Pt clusters (see also CVs). For a more detailed discussion of the band assignment, we refer to our previous work.[28]

For C2-150-O2 we also observe the $CO_t$ band at 2039 $cm^{-1}$, however, the band at 2103 $cm^{-1}$ and the band assigned to bridge bonded CO are missing. The shape as well as the evolution of the $CO_t$ band is quite similar to the sample conditioned in C2-150-Ar, with slightly lower band intensities of the band assigned to the small Pt clusters, in line with our observations by CV. In the IRRA spectra of the sample treated with R-800-Ar, we observe only contributions from $CO_t$, however, with a different shape. At 0.05 $V_{RHE}$, the peak shape is dominated by the contributions assigned to adsorption on Pt facets (2055 $cm^{-1}$) and Pt atoms neighboring the alloying metals (2007 $cm^{-1}$), which are oxidized at ~0.6 $V_{RHE}$. Above 0.6 $V_{RHE,}$ the intensity of the remaining band assigned to the Pt clusters is much lower than on the other samples.

In Figure 7d, we provide the comparison of the IRRA spectra of the different samples at 0.05 $V_{RHE}$, highlighting the differences. The sample conditioned in C2-150-O2, which has the highest specific activity for ORR, shows, in contrast to the reference sample, a pronounced contribution of small Pt clusters (2039 $cm^{-1}$). On the other hand, it does not show any $CO_b$ signal as observed for the sample conditioned under C2-150-Ar. Note that $CO_b$ is preferentially observed on larger particle, which have larger facets.[40] We speculate that larger particles form especially during the conditioning in C2-150-Ar due to Ostwald ripening and/or coalescence.

A STEM-EDXS study of pristine and C2-150-Ar conditioned catalysts was carried out. Octahedral shaped 4–7 nm nanoparticles are evident for the pristine catalyst, which restructure to roundish shaped 4–7 nm nanoparticles after C2-150-Ar conditioning (see Supporting Information Figure S1, S3 and S4). Elemental maps of the aged catalysts showed remarkably reduced Nickel signal compared to the pristine catalysts, indicating a plausible Pt leaching during C2-150-Ar conditioning process (Figure 8). Careful checking of the acquired Z-contrast image showed that very small metal clusters below 1.5 nm in size are observable for the C2-150-Ar conditioned catalysts (Supporting Information S5). Small cluster can also be found in the pristine catalyst but seem to be in lower amount. Nevertheless, this HAADF study is a very local one and quantitative information shall not be deduced from this. Clearly, the study corroborates the EC-IRRAS findings, which provide information averaged over a large area.

Dissolution and redeposition might be a driving force for the catalyst changes, as seen in our previous study. In that study, scanning flow cell inductively coupled plasma mass spectrometry (SFC-ICP-MS) was carried out for the first conditioning cycles.[28] Dissolution was observed, however, for Pt

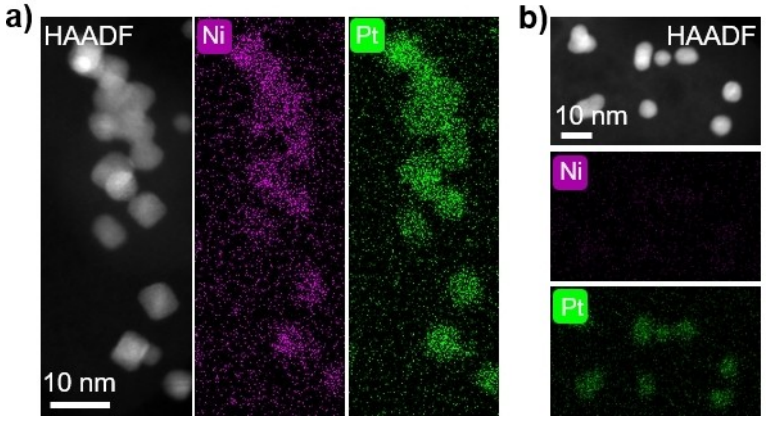


**Figure 8.** Elemental maps of a) pristine PtNiMo/C catalyst and b) after C2-150-Ar preconditioning.

and Mo the signal intensities were close to the detection limit. To improve the quality of the data in this study, we accumulated the dissolved species over time within the electrolyte and subsequently determined the concentration of the dissolved species by ICP-MS. This was done for the conditionings C2-150-N2 as well as R-800-N2 and additional subsequent 10 ORR cycles in fresh electrolyte, as shown in Figure S14 in the Supporting Information. For the conditioning R-800-N2 approx. 34% of the initial Ni was leached and a small amount of Pt (0.6%). Also, Mo leaching is detected but is due to the low initial Mo amount close to the detection limit. The detected leached amount would correspond to 180% of the initial Mo content. The unrealistic number stems from the detection limit during the leaching experiment as well as the error for determining the very low initial Mo amount, which is only 0.04 wt.-% of the catalyst (including carbon). Thus, quantitative discussions for the leached Mo amount shall be avoided. After electrolyte refreshing and additional 10 ORR cycles a more pronounced platinum leaching can be observed in parallel to an also pronounced Ni and Mo leaching. In numbers during the 10 ORR cycles 3.3% of the initial Pt, 10.5% of the initial Ni and 85% of the initial Mo was additionally leached. For the C2-150-N2 conditioning similar but for Pt slightly lower numbers result. After the conditioning 0.51% of the Pt and after the subsequent 10 ORR cycles in fresh electrolyte additional 2.25% were leached. Thus, in total the amount of Pt leached during R-800-N2 is a factor of 1.4 higher compared to the C2-150-N2 conditioning. For Ni the leaching is more similar, and the factor is only 1.08.

Based on all insights we propose that the alternative conditioning protocols studied by us, allow that leached Pt during the conditioning is redeposited more and especially small active Pt clusters are created during these redeposition. During a classical pretreatment and ORR activity measurement more leached Pt is lost and bigger nanoparticles are redeposited. This study cannot rule out that during this different restructuring processes other highly active sites are formed e.g., in small amount, which also are responsible for the observed activity differences.

### Stability of Higher Activity Resulting from New Conditioning Protocols

If a high amount of small Pt clusters is the reason for the increased activity when employing Conditioning 2 and 3 as protocol despite the reference, the question remains, if these high activities can be maintained also for a longer time. To answer this question, accelerated degradation tests (ADT) with cycling between 0.60–1.10 $V_{RHE}$ at 50 mV $s^{-1}$ in $N_2$ were carried out and the activity was determined prior to the ADT and after 8,000, 16,000 and 24,000 ADT cycles. Again additional 45 ORR cycles with three times electrolyte refreshing were employed to assess the activity before and after the ADT. As conditioning protocols, the Conditioning 2 with 150 cycles in $O_2$ (C2-150-O2), the chronoamperometric Conditioning 3 with 300 steps between 0.70–1.00 $V_{RHE}$ (C3-300-N2) and the Reference Conditioning (R-800-N2) were chosen.

The results of the polarization curves are given in the Supporting Information (Figure S10) and summarized in Figure 9. For all conditionings the results prior to the ADT are similar to the insights obtained before. For both C2-150-O2 and R-800-N2 stable activities are obtained, while Conditioning 2 results in higher activities. For C3-300-N2 strong activity changes are observed, and steady activity is not reached yet (Figure 9b). Nevertheless, after 8k ADT cycles a very similar behavior is seen for all three conditionings. Always between the 1st and 16th additional ORR cycles an activity increase is seen and afterwards from the 16th and 31st cycle the activity stays constant. These behavior points to the necessity to apply the protocol developed in this work to determine reliable steady state activities, as the first ORR cycles are obviously biased. Subsequently the activity was deduced as average of the 16th and 31st additional cycle. Comparing the steady state activities gained for the 16th and 31st additional ORR cycle after 8k ADT cycles, the catalyst after C3-300-N2 shows the highest activity of 1.77 mA $cm_{Pt}^{-2}$, followed by 1.28 mA $cm_{Pt}^{-2}$ for C2-150-O2 and 0.72 mA $cm_{Pt}^{-2}$ for R-800-N2. Nevertheless, the catalyst with conditioning C3-300-N2 shows also stronger deactivation from 8 k to 16 k ADT cycles with 18% of SA loss followed by a less pronounced loss from 16 k to 24 k ADT cycles. After 24 k cycles the SA for C3-300-N2 is 1.31 mA $cm_{Pt}^{-2}$ and still a factor of 1.71 higher compared to the Reference Conditioning (Figure 9c) after 24 k cycles. For C2-150-O2 (Figure 9a) the activity is also always higher than the reference. A slight deactivation of 5.6% of SA from 8 k to 16 k ADT cycles is observed, which shows that the catalyst finished equilibration during the conditioning. A loss of 5.9% of SA follows from 16 k to 24 k. After 24 k still an activity of 1.10 mA $cm_{Pt}^{-2}$ results which is a factor of 1.44 higher compared to the Reference Conditioning after 24 k ADT cycles results.

## Conclusions

Our study showed that the conditioning has a pronounced influence on the ORR activity of the state–of–the–art Pt-based catalysts. The commonly employed CV scans with 500 mV $s^{-1}$ results in a lower activity of 0.82 mA $cm^{-2}$ at 0.95 $V_{RHE}$, while a slower scan rate of 20 mV $s^{-1}$ results in initial activities of approx. 1.25 mA $cm^{-2}$. The study showed also that determining these initial activities after catalyst equilibration is not a facile task and a new protocol was presented which combines three times electrolyte refreshment with 15 additional ORR cycles each. When the ORR activity for the last two electrolyte refreshments is constant, the equilibration of catalyst is finished, and initial activities can be determined. The ex–situ and in–situ characterization methods allowed us to deduce a mechanism for the strong activity dependency on the preconditioning. During the conditioning the known Ni but also Pt leaching takes place. Slow conditioning leads to a partial redeposition of Pt forming small sized clusters and probably single atoms, which exhibit high activity. For the fast condition the number of

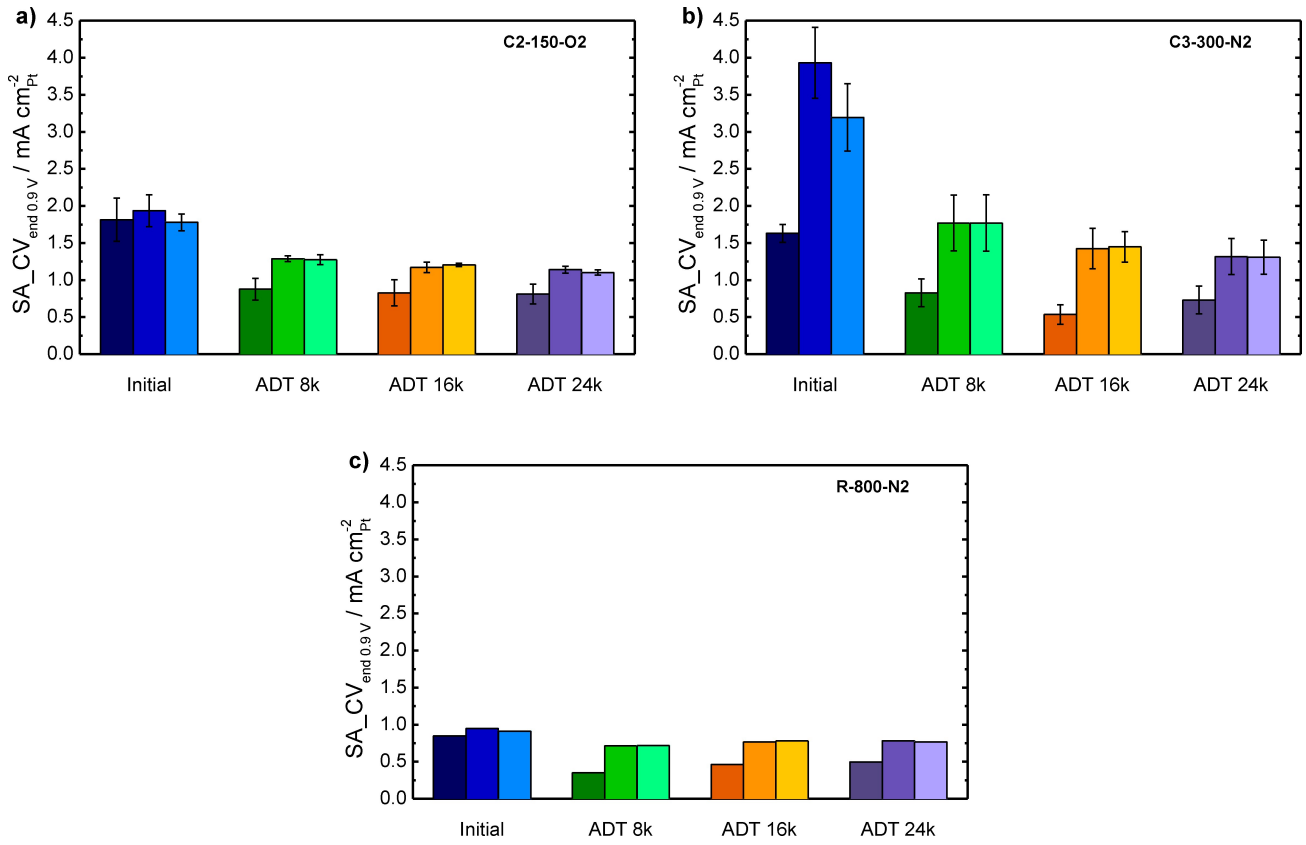


**Figure 9.** Activity recordings after conditioning with a) C2-150-O2, b) C3-300-N2 and c) R-800-N2 as initial activities and after 8,000, 16,000 and 24,000 ADT-cycles, respectively. Shown are the activity at the 1st, 16th and 31st ORR-cycle after electrolyte refreshing. ADT in potential range of 0.6–1.1 $V_{RHE}$ at 50 mV $s^{-1}$ in $N_2$, SA record at 0.9 $V_{RHE}$ between 0.05–1.20 $V_{RHE}$ with 20 mV $s^{-1}$ and 1600 rpm rotation speed in $O_2$-saturated 0.1 M $HClO_4$ solution.

small clusters and single atoms is comparable lower. Obviously, the time scale of the reductive / oxidative cycling needs to match the nucleation and growth dynamics of the Pt clusters to generate new highly active sites from the leached Pt. Interestingly, an increased activity can even be leveraged after an accelerated stress test of 24,000 cycles from 0.6 to 1.10 $V_{RHE}$ showing that the newly created active sites also show pronounced stability.

## Experimental Section

### Materials

$Pt(acac)_2$ (98%) and $Mo(CO)_6$ (98%) were purchased from Acros Organics. $Ni(acac)_2$ (95%) was purchased from Sigma–Aldrich. Perchloric acid (70%) was purchased from Carl Roth. *N*,*N*-Dimethylformamide (99.8+%) was obtained from Alfa Aesar. Benzoic acid (99%) was obtained from Merck Millipore. Deionized water (< 1.0 μS $cm^{-1}$) from VWR chemicals or ultrapure water (Milli-Q Synergy UV, 18.2 MΩ·cm at 298 K, TOC < 5 ppb) were used for preparation of aqueous solutions. All chemicals were used as received without further purification.

### Synthesis of PtNiMo/C Catalyst

The synthesis of carbon supported PtNiMo catalyst was performed using a solvothermal method following free of bulky capping agents described in literature.[29,41] Detailed information on the synthesis can be found in the Supporting Information. As reported prior[28] the catalyst consists of octahedral shaped PtNiMo nanoparticles with an overall particle size of approx. 6.0 nm (Figure S1 and S2). ICP-OES analysis determined a Pt-loading of 22.2 wt.% and a final atomic composition of Pt:Ni:Mo = 1:0.61:0.0035. For further characterization of catalyst after this specific synthesis method we refer to our previous publications.[25,28]

### Instrumentation

The determination of the exact loadings of Pt, Ni and Mo on the catalyst samples were done using inductively coupled plasma optical emission spectroscopy (ICP-OES, Optima 2000DV, *PerkinElmer*). The powder X-ray diffraction (XRD) patterns are measured on a StadiP (*Stoe*) using a Ge(111) monochromator with Cu K$\alpha$ radiation ($\lambda$ = 1.54060 Å). STEM images were recorded using a Thermo Fisher Scientific (TFS) double Cs- corrected Titan Themis3 TEM operating at 300 kV. Further information is given in Supporting Information.

### Electrochemical Measurements

The electrochemical measurements were carried out on an OctoStat5000 multichannel potentiostat (*IVIUM Technologies*), which is controlled by IviumSoft. As counter (CE) and reference (RE) electrodes, a graphite rod (*PINE*) and a leak–free double–junction 3 M KCl Ag/AgCl electrode (*Aldrich*) were used, respectively. All potentials reported here were calibrated against the reversible hydrogen electrode (RHE), if not declared otherwise. A glassy–

carbon rotating disk electrode (GC-RDE, 5 mm diameter, *PINE*) was used as the working electrode (WE). All glass and Teflon ware and all noble metal wires used for in situ measurements, were stored in a solution of NOCHROMIX (Sigma–Aldrich) in concentrated sulfuric acid (Merck, Emsure, 98%). Prior to each experiment, the equipment was rinsed five times with ultrapure water (Milli–Q Synergy UV, 18.2 MΩ·cm at 298 K, TOC < 5 ppb) and subsequently boiled three times in Milli–Q water for at least 30 min. The RDE was polished on a pad with 0.3 μm alumina polishing solution and cleaned ultrasonically with acetone, ethanol and deionized water to remove contaminations. 2 mL catalyst ink was prepared by sonicating a suspension of the PtNiMo/C catalyst powder in a mixture of 3:1 ethanol:deionized water and 5% Nafion. The ionomer/carbon ratio was set at 0.55 $g\,g^{-1}$ for all measurements. Furthermore, a calibrated amount of catalyst ink for a 2 μg Pt loading (10 $\mu g_{Pt}\,cm^{-2}$) based on the RDE geometric area was applied onto the RDE and dried under argon flow. All electrochemical measurements were performed at room temperature in $N_2$ or $O_2$ saturated 0.1 M $HClO_4$ solution and in the potential range of 0.05–1.20 $V_{RHE}$. The ECSA value was determined by measuring the H adsorption charge from the cyclic voltammetry (CV) curves at 20 $mV\,s^{-1}$. For calibration, 210 $\mu C\,cm_{Pt}^{-2}$ were used as charge density for polycrystalline platinum.[2] Furthermore, a chronoamperometric method with 300 square–wave potential steps between 0.60/0.65/0.70 $V_{RHE}$ to 1.00 $V_{RHE}$ and a dwell time of 57.5 sec at each step was chosen, respectively. In the accelerated durability test (ADT), the samples were cycled over 8,000, 16,000, and 24,000 cycles between 0.60 to 1.10 $V_{RHE}$ at 50 $mV\,s^{-1}$ in $N_2$ saturated electrolyte, respectively. ORR measurements were carried out recording polarization curves in $O_2$ saturated 0.1 M $HClO_4$ solution at 20 $mV\,s^{-1}$ and a rotation of 1600 rpm. Prior to each ORR activity measurement, the electrolyte was purged for a minimum of 20 min with high purity oxygen and an $O_2$ flow was maintained to avoid any disturbance from ambient atmosphere during the measurements. Further information on the electrochemical measurements is summarized in the Supporting Information.

## Catalyst conditioning

As different conditioning methods for the PtNiMo/C catalyst, the following method protocols were applied, which are illustrated in Scheme 1:

- Conditioning 1: First, 0.1 M $HClO_4$ electrolyte was flushed for 20 min with $N_2$ while holding the working electrode at open circuit potential (OCP). Subsequently, a fast start up from 0.05 to 1.20 $V_{RHE}$ with 500 $mV\,s^{-1}$ in $N_2$ for 10 or 15 cycles were carried out. This method is always followed by Conditioning 2.
- Conditioning 2: A new electrolyte was saturated with $N_2$ or $O_2$ for 20 min and the working electrode was placed into it, which was either previously treated with the Conditioning 1 method or not. Afterwards, 100 or 150 cycles at 20 $mV\,s^{-1}$ in $N_2$ or $O_2$ between 0.05 to 1.20 $V_{RHE}$ were carried out, respectively.
- Conditioning 3: The chronoamperometric method was carried out by first flushing the electrolyte with $N_2$ for 20 min and subsequently placing the working electrode into it. 300 square wave potentials were recorded between 0.60, 0.65 and 0.70 $V_{RHE}$ as lower limits and 1.00 $V_{RHE}$ as upper limit at a dwell time of 57.5 sec at each step, respectively.
- Reference: The electrolyte was saturated for 20 min with $N_2$, while holding the working electrode at OCP. The measurement was carried out with 800 cycles at 500 $mV\,s^{-1}$ in $N_2$ between 0.05 to 1.20 $V_{RHE}$.

Three different protocols to determine ORR activity were studied and different combinations of ORR polarization curves with recording an anodic linear sweep voltammetry (LSV) under 1600 rpm rotation at 20 $mV\,s^{-1}$ between 0.05 to 1.20 $V_{RHE}$:

- The first activity determination employed flushing the electrolyte for 20 min with $O_2$ while holding the working electrode at OCP. Afterwards, 10 LSVs were recorded, the working electrode rotation was stopped and the working electrode was placed into a fresh $O_2$ saturated electrolyte. Subsequently, 10 more LSV cycles under rotation were recorded.

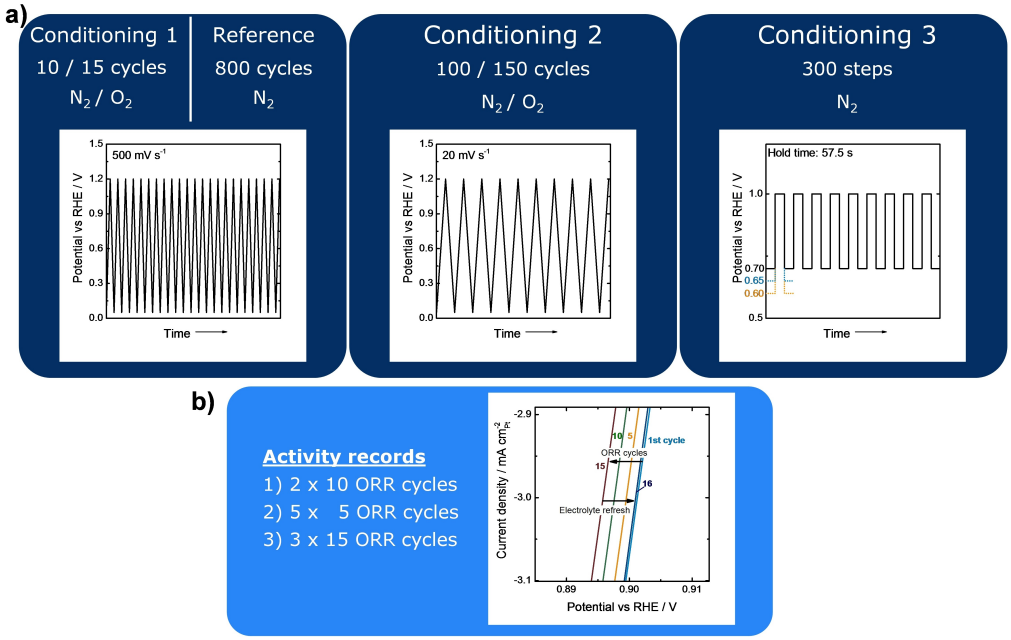


**Scheme 1.** Protocol for conditioning and activity records of PtNiMo/C catalyst. a) Four different possible pre–treatments: Reference method is defined for 800 cycles at 500 $mV\,s^{-1}$ in $N_2$; Conditioning 1 at 500 $mV\,s^{-1}$, Cond 2 at 20 $mV\,s^{-1}$ in $N_2$ or $O_2$ and Cond 3 300 square wave potential steps, respectively. b) Activity records after conditioning in three different methods: 1) 10 cycles of LSV for ORR, refreshing electrolyte and additional 10 cycles. 2) 5 LSV cycles, electrolyte refresh and repeating in total five times. 3) 15 LSV cycles, refreshing electrolyte and repeating in total three times. Potential range: 0.05–1.20 $V_{RHE}$, ORR at 20 $mV\,s^{-1}$ and 1600 rpm rotation in $O_2$-saturated 0.1 M $HClO_4$ solution.

- The second activity determination was carried out as described above, but using 5 LSV cycles in $O_2$, refreshing the electrolyte by placing the working electrode into a new solution and repeating the 5 LSV cycles. In total 5 times 5 LSV repetitions were carried out.
- The third activity method was recorded by using 15 LSV cycles in $O_2$, refreshing the electrolyte and repeating in total three times 15 LSV cycles.

### CO-Stripping Measurements

CO stripping – cyclic voltammetry: We measured CVs in hanging meniscus configuration[42] in 0.1 M $HClO_4$ (Carl Roth, ROTIPURAN Ultra) with a three–electrode setup. We deposited catalyst ink on a bead–type gold electrode. A gold wire was used as CE and a RHE as RE. We used a commercial potentiostat (Gamry, Reference [600]) and controlled the potential throughout the entire measurement. We treated the samples by recording 150 CVs (treatment Conditioning 2) in inert gas (C2-150-Ar) or $O_2$ (C2-150-O2) between 0.05 and 1.2 $V_{RHE}$ at a scan rate of 20 $mV\,s^{-1}$. As a reference (treatment Reference) we recorded 800 cycles in the identical potential window at a scan rate of 500 $mV\,s^{-1}$ (R-800-Ar). Subsequently, we adsorbed CO at 0.05 $V_{RHE}$ for 2 min and purged the solution with Ar for 10 min to remove all dissolved CO. Finally, we recorded a CV between 0.05 and 1.2 $V_{RHE}$ at a scan rate of 20 $mV \cdot s^{-1}$.

CO stripping — electrochemical in-situ IR spectroscopy: To measure EC-IRRAS we used a commercial IR spectrometer with evacuated optics (Bruker Vertex 80v) and a liquid nitrogen cooled mercury cadmium telluride (MCT) narrow band detector. The spectrometer was equipped with a commercial optics for electrochemical measurements, a home—built electrochemical cell and a polarizer. We used a $CaF_2$ hemisphere (Korth) as IR transparent window material sealed with a Kalrez gasket. We controlled the potential with a commercial potentiostat (Gamry Reference [600]). We deposited the catalyst ink on a gold substrate with a surface area of 1.1 $cm^2$. We used an Au wire as the counter electrode and a home build RHE as RE. Spectra were measured with p-polarized light. First, we recorded CV in a retracted position following the procedure described in CO stripping—cyclic voltammetry. Afterwards, CO (Linde 4.7) was adsorbed at 0.05 $V_{RHE}$ for 2 min. Subsequently we purged the solution with Ar for 10 min. We increased during the measurement stepwise the potential from 0.05 to 1.2 $V_{RHE}$ in 0.1 V steps. At each step, we acquire IR spectra with 128 scans per spectrum, a resolution of 2 $cm^{-1}$, and an acquisition time of 57 s. IR measurements were performed in a thin layer configuration. For a more detailed description of the IR setup used, we refer to literature.[43]

## Supporting Information

The authors have cited additional references within the Supporting Information.[6,11,12,15,17,22,25,28,29,41,44,45,46,47,48,49,50]

## Acknowledgements

B.E. acknowledge the funding from the European Research Council (ERC) under the European Union's Horizon2020 research and innovation program (grant agreement No. 681719). BE acknowledges the support by the Bavarian State Ministry for Science and Arts through the Distinguished Professorship Program. J. L., K. M. E. S., M. W. and Z. X., acknowledge financial support by the Deutsche Forschungsgemeinschaft (DFG) via Collaborative Research Centre SFB 1452—Catalysis at Liquid Interfaces (project 431791331). O. B. acknowledges financial support by the DFG via the project 431733372. J. Y. acknowledges the support provided by the China Scholarship Council (CSC). M. L. acknowledges the Federal Ministry of Education and Research (BMBF) in the framework of NanoMatFutur (SynKat, FK: 03XP0265) for financial support. K. J. J. M., D. D. and P. L. D. thank the German Ministry of Education and Research (BMBF) for financial support within the project 03HY108 A. G.-R. Z. acknowledges the funding from the National Natural Science Foundation of China (NSFC, No. 22272117) and the National Key R&D Program of China (No. 2023YFB4004700). Open Access funding enabled and organized by Projekt DEAL.

## Conflict of Interests

The authors declare no conflict of interest.

## Data Availability Statement

The data that support the findings of this study are openly available in Zenodo at https://doi.org/10.5281/zenodo.10557038, reference number 10557038.

**Keywords:** Accelerated Durability · Cyclic Voltammetry · Nanoparticles · Oxygen Reduction · Pretreatment

[1] L. Huang, S. Zaman, X. Tian, Z. Wang, W. Fang, B. Y. Xia, *Acc. Chem. Res.* **2021**, *54*, 311–322.
[2] H. A. Gasteiger, S. S. Kocha, B. Sompalli, F. T. Wagner, *Appl. Catal. B* **2005**, *56*, 9–35.
[3] J. C. Meier, C. Galeano, I. Katsounaros, J. Witte, H. J. Bongard, A. A. Topalov, C. Baldizzone, S. Mezzavilla, F. Schüth, K. J. J. Mayrhofer, *Beilstein J. Nanotechnol.* **2014**, *5*, 44–67.
[4] E. Pizzutilo, S. Geiger, J. P. Grote, A. Mingers, K. J. J. Mayrhofer, M. Arenz, S. Cherevko, *J. Electrochem. Soc.* **2016**, *163*, F1510–F1514.
[5] A. S. B. Federico Calle-Vallejo, Jakub Tymoczko, Viktor Colic, Quang Huy Vu, Marcus D. Pohl, Karina Morgenstern, David Loffreda, Philippe Sautet, Wolfgang Schuhmann, *Science* **2015**, *350*, 185–190.
[6] P. Strasser, S. Koh, T. Anniyev, J. Greeley, K. More, C. Yu, Z. Liu, S. Kaya, D. Nordlund, H. Ogasawara, *Nat. Chem.* **2010**, *2*, 454.
[7] V. R. Stamenkovic, B. Fowler, B. S. Mun, G. Wang, P. N. Ross, C. A. Lucas, N. M. Marković, *Science (1979)* **2007**, *315*, 493–497.
[8] P. Strasser, M. Gliech, S. Kuehl, T. Moeller, *Chem. Soc. Rev.* **2018**, *47*, 715–735.
[9] V. R. S. Chen Chen, Yijin Kang, Ziyang Huo, Zhongwei Zhu, Wenyu Huang, Huolin L. Xin, Joshua D. Snyder, Dongguo Li, Jeffrey A. Herron, Manos Mavrikakis, Miaofang Chi, Karren L. More, Yadong Li, Nenad M. Markovic, A. S. Gabor, C. Chen, *Science (1979)* **2014**, *343*, 1339–1343.
[10] S. Polani, K. E. MacArthur, M. Klingenhof, X. Wang, P. Paciok, L. Pan, Q. Feng, A. Kormányos, S. Cherevko, M. Heggen, P. Strasser, *ACS Catal.* **2021**, 11407–11415.
[11] C. Cui, L. Gan, M. Heggen, S. Rudi, P. Strasser, *Nat. Mater.* **2013**, *12*, 765–771.
[12] C. Cui, M. Ahmadi, F. Behafarid, L. Gan, M. Neumann, M. Heggen, B. R. Cuenya, P. Strasser, *Faraday Discuss.* **2013**, *162*, 91–112.
[13] V. R. Stamenkovic, B. S. Mun, M. Arenz, K. J. J. Mayrhofer, C. A. Lucas, G. Wang, P. N. Ross, N. M. Markovic, *Nat. Mater.* **2007**, *6*, 241–247.
[14] V. R. Stamenkovic, B. S. Mun, K. J. J. Mayrhofer, P. N. Ross, N. M. Markovic, *J. Am. Chem. Soc.* **2006**, *128*, 8813–8819.

[15] S. Kühl, M. Gocyla, H. Heyen, S. Selve, M. Heggen, R. E. Dunin-Borkowski, P. Strasser, *J. Mater. Chem. A. Mater.* **2019**, *7*, 1149–1159.
[16] R. Chattot, I. Martens, M. Scohy, J. Herranz, J. Drnec, F. Maillard, L. Dubau, *ACS Energy Lett.* **2020**, *5*, 162–169.
[17] F. Dionigi, C. C. Weber, M. Primbs, M. Gocyla, A. M. Bonastre, C. Spöri, H. Schmies, E. Hornberger, S. Kühl, J. Drnec, *Nano Lett.* **2019**, *19*, 6876–6885.
[18] P. J. Ferreira, G. J. la O', Y. Shao-Horn, D. Morgan, R. Makharia, S. Kocha, H. A. Gasteiger, *J. Electrochem. Soc.* **2005**, *152*, A2256.
[19] J. Knossalla, P. Paciok, D. Göhl, D. Jalalpoor, E. Pizzutilo, A. M. Mingers, M. Heggen, R. E. Dunin-Borkowski, K. J. J. Mayrhofer, F. Schüth, *J. Am. Chem. Soc.* **2018**, *140*, 15684–15689.
[20] J. Lu, L. Luo, S. Yin, S. W. Hasan, P. Tsiakaras, *ACS Sustainable Chem. Eng.* **2019**, *7*, 16209–16214.
[21] S. Feng, J. Lu, L. Luo, G. Qian, J. Chen, H. S. Abbo, S. J. J. Titinchi, S. Yin, *J. Energy Chem.* **2020**, *51*, 246–252.
[22] Q. Jia, Z. Zhao, L. Cao, J. Li, S. Ghoshal, V. Davies, E. Stavitski, K. Attenkofer, Z. Liu, M. Li, X. Duan, S. Mukerjee, T. Mueller, Y. Huang, *Nano Lett.* **2018**, *18*, 798–804.
[23] R. M. Arán-Ais, F. Dionigi, T. Merzdorf, M. Gocyla, M. Heggen, R. E. Dunin-Borkowski, M. Gliech, J. Solla-Gullón, E. Herrero, J. M. Feliu, *Nano Lett.* **2015**, *15*, 7473–7480.
[24] N. Erini, V. Beermann, M. Gocyla, M. Gliech, M. Heggen, R. E. Dunin-Borkowski, P. Strasser, *Angew. Chem. Int. Ed.* **2017**, *56*, 6533–6538.
[25] M. George, G.-R. Zhang, N. Schmitt, K. Brunnengräber, D. J. S. Sandbeck, K. J. J. Mayrhofer, S. Cherevko, B. J. M. Etzold, *ACS Catal.* **2019**, *9*, 8682–8692.
[26] V. Stamenkovic, B. S. Mun, K. J. J. Mayrhofer, P. N. Ross, N. M. Markovic, J. Rossmeisl, J. Greeley, J. K. Nørskov, *Angew. Chem.* **2006**, *118*, 2963–2967.
[27] J. K. Nørskov, J. Rossmeisl, A. Logadottir, L. Lindqvist, J. R. Kitchin, T. Bligaard, H. Jonsson, *J. Phys. Chem. B* **2004**, *108*, 17886–17892.
[28] B. Danisman, G.-R. Zhang, A. F. Baumunk, J. Yang, O. Brummel, P. Darge, K. J. J. Mayrhoferhttps, J. Libuda, M. Ledendecker, B. J. M. Etzold, *ChemElectroChem.* **2023**, *10*, e202300109.
[29] X. Huang, Z. Zhao, L. Cao, Y. Chen, E. Zhu, Z. Lin, M. Li, A. Yan, A. Zettl, Y. M. Wang, *Science (1979)* **2015**, *348*, 1230–1234.
[30] R. K. Ahluwalia, J.-K. Peng, X. Wang, D. A. Cullen, A. J. Steinbach, *J. Electrochem. Soc.* **2017**, *164*, F306–F320.
[31] S. Rudi, C. Cui, L. Gan, P. Strasser, *Electrocatalysis* **2014**, *5*, 408–418.
[32] F. Maillard, S. Schreier, M. Hanzlik, E. R. Savinova, S. Weinkauf, U. Stimming, *Phys. Chem. Chem. Phys.* **2005**, *7*, 385–393.
[33] F. Maillard, M. Eikerling, O. V. Cherstiouk, S. Schreier, E. Savinova, U. Stimming, *Faraday Discuss.* **2004**, *125*, 357–377.
[34] I. Villegas, M. J. Weaver, *J. Chem. Phys.* **1994**, *101*, 1648–1660.
[35] O. Brummel, F. Waidhas, I. Khalakhan, M. Vorokhta, M. Dubau, G. Kovács, H. A. Aleksandrov, K. M. Neyman, V. Matolín, J. Libuda, *Electrochim. Acta* **2017**, *251*, 427–441.
[36] L. DeRita, S. Dai, K. Lopez-Zepeda, N. Pham, G. W. Graham, X. Pan, P. Christopher, *J. Am. Chem. Soc.* **2017**, *139*, 14150–14165.
[37] H. V. Thang, G. Pacchioni, L. DeRita, P. Christopher, *J. Catal.* **2018**, *367*, 104–114.
[38] T. Iwasita, F. C. Nart, *Prog. Surf. Sci.* **1997**, *55*, 271–340.
[39] O. Brummel, F. Waidhas, F. Faisal, R. Fiala, M. Vorokhta, I. Khalakhan, M. Dubau, A. Figueroba, G. Kovács, H. A. Aleksandrov, G. N. Vayssilov, S. M. Kozlov, K. M. Neyman, V. Matolín, J. Libuda, *J. Phys. Chem. C* **2016**, *120*, 19723–19736.
[40] F. Faisal, C. Stumm, M. Bertram, T. Wähler, R. Schuster, F. Xiang, O. Lytken, I. Katsounaros, K. J. J. Mayrhofer, M. A. Schneider, *Phys. Chem. Chem. Phys.* **2018**, *20*, 23702–23716.
[41] M. K. Carpenter, T. E. Moylan, R. S. Kukreja, M. H. Atwan, M. M. Tessema, *J. Am. Chem. Soc.* **2012**, *134*, 8535–8542.
[42] C. Korzeniewski, V. Climent, J. Feliu, *Electroanalytical chemistry: A series of advances* **2011**, *24*, 75–170.
[43] F. Faisal, M. Bertram, C. Stumm, F. Waidhas, O. Brummel, J. Libuda, *Rev. Sci. Instrum.* **2018**, *89*, DOI 10.1063/1.5047056.
[44] Y. Garsany, O. A. Baturina, K. E. Swider-Lyons, S. S. Kocha, *Anal. Chem.* **2010**, *82 (15)*, 6321–6328.
[45] K. J. J. Mayrhofer, D. Strmcnik, B. B. Blizanac, V. Stamenkovic, M. Arenz, N. M. Markovic, *Electrochim. Acta* **2008**, *53*, 3181–3188.
[46] B. A. Pinaud, A. Bonakdarpour, L. Daniel, J. Sharman, D. P. Wilkinson, *J. Electrochem. Soc.* **2017**, *164*, F321–F327.
[47] Y. Garsany, J. Ge, J. St-Pierre, R. Rocheleau, K. E. Swider-Lyons, *J. Electrochem. Soc.* **2014**, *161*, F628.
[48] S. S. Kocha, K. Shinozaki, J. W. Zack, D. J. Myers, N. N. Kariuki, T. Nowicki, V. Stamenkovic, Y. Kang, D. Li, D. Papageorgopoulos, *Electrocatalysis* **2017**, *8*, 366–374.
[49] S. Kühl, H. Heyen, P. Strasser, *ECS Trans.* **2016**, *75*, 723.
[50] X. Tan, S. Prabhudev, A. Kohandehghan, D. Karpuzov, G. A. Botton, D. Mitlin, *ACS Catal.* **2015**, *5*, 1513–1524.

Manuscript received: January 24, 2024
Revised manuscript received: February 26, 2024
Version of record online: March 20, 2024